Kufa Journal of Engineering
Vol. 17, No. 3, July 2026, P.P. 652-664
Article history: Received 1 December 2025, last revised 9 January 2026, accepted 10 January 2026

CHARACTERIZING POLARIZATION-BASED DESIGNS OF UNBALANCED MACH-ZEHNDER INTERFEROMETERS

Saif A. Al Graiti[1] and Saif A. Jasim[2]

[1] IT Research and Development Center, University of Kufa, Najaf, Iraq, Email:saif.jasim@uokufa.edu.iq.

[2] Department of Electronic and Communications Engineering, Faculty of Engineering, University of Kufa, Najaf, Iraq, Email:saifa.halboos@uokufa.edu.iq.

https://doi.org/10.30572/2018/KJE/170337

ABSTRACT

We have experimentally investigated and simulated the diversity of unbalanced Mach-Zehnder interferometer (UMZI) designs. The group index and free spectral range (FSR) are measured for both the transverse electric (TE) and transverse magnetic (TM) designs for a silicon (Si) strip waveguide that has a 500 nm width and a 220 nm height. The simulated TE UMZI with arm's length difference of 50 µm shows 11 nm and 4.33 of the FSR and group index, respectively. The group index is 3.103, and FSR is 13.5 for the TM UMZI. These designs show a slight variation compared with the simulation results due to fabrication variation. Overall, the TM UMZI design is more sensitive to the manufacturing variation than the TE UMZI designs. Photonic interferometers have been widely used in photonic devices, and such photonic devices have potential applications in photonic modulators, sensors, filters, and future computing via photonic integrated circuits (PICs).

KEYWORDS

Photonic Integrated Circuits (PICs), Mach-Zehnder Interferometer, Fee Spectral Range Refractive Index, Group Index, electron beam lithography, Optical Computing.

1. INTRODUCTION

Photonic devices play a potential role in high-speed optoelectronic applications (Chrostowski and Hochberg, 2015). In addition to high-speed capability, photonic devices are compact in size via photonic integrated circuit systems (PICs); such applications include photonic communication and computing (Chrostowski and Hochberg, 2015, Chrostowski and Shoman, 2021, Saini et al., 2019, Saghaei, Elyasi and Karimzadeh, 2019, Tapia-Licona et al., 2025) and microwave photonic filters (AL-Zaidi, 2025). A Mach-Zehnder interferometer (MZI) is a basic platform device for several applications, such as optical modulators and optical sensing applications (Chrostowski and Hochberg, 2015, Chrostowski and Shoman, 2021, Saini et al., 2019, Saghaei, Elyasi and Karimzadeh, 2019). Previously, Mach-Zehnder interferometers (MZIs) have been widely used in communications applications as electro-optic modulators (Chrostowski and Hochberg, 2015). Thermo-optical switches are studied with 540 µW switching power, 141 µs rise time, and a 25 dB extinction ratio via the unbalanced MZIs (Sun and Reano, 2010). A thermo-optical switch with crosstalk of 50 dB 2 x 2 is achieved using an array of MZIs (Shoji et al., 2010). A traveling wave electrode-based MZI silicon optical modulator is demonstrated with 50 Gb/s (Tu et al., 2013). A photonic biosensor is reported based on silicon nitride slot waveguides in MZI structure (Liu et al., 2013).

The UMZI structure works based on interference phenomena (Chrostowski and Hochberg, 2015, Chrostowski and Shoman, 2021, Saini et al., 2019, Saghaei, Elyasi and Karimzadeh, 2019). The input optical signal enters the 3-dB Y-branch to equally split the optical signal into the two arms of the UMZI as in Fig. 1 (a). Then, the optical signals merge again at the 3-dB coupler after propagation through the two arms. The length difference between the two arms causes a phase difference between the optical signals in the two paths (upper and lower arms); thus, an interference occurs. The output power coming out of the 3- dB coupler (combiner) exhibits a sinusoidal behavior due to the constructive and destructive interferences.

The design cycle of a UMZI structure undergoes four main stages as shown in Fig. 1(b), first modeling and simulation when mathematical expressions are derived and circuit simulation is conducted. In the second stage, KLayout is used to draw the UMZI designs. Then, the design rule check is performed in KLayout to find and fix errors to send to the fabrication facility, as in the third stage. Then, designs are tested using a PIC test station. Testing is achieved at the wafer level to measure the design and compare results with the modeling and simulation. All of these stages are investigated in this work.

Previous studies focused on investigating UMZ structure with different arms for the TE mode (Saghaei, Elyasi and Karimzadeh, 2019, El Shamy et al., 2022, and Ndamati, Olayemi and

Madu, 2024). These studies characterize the FSR for different structures of the UMZI, but lack a full analysis of the group index analysis. The group index analysis is essential for further investigation of group velocity and dispersion that might affect the performance of high-performance applications in PICs. Furthermore, these studies focus on TE based UMZI structure.

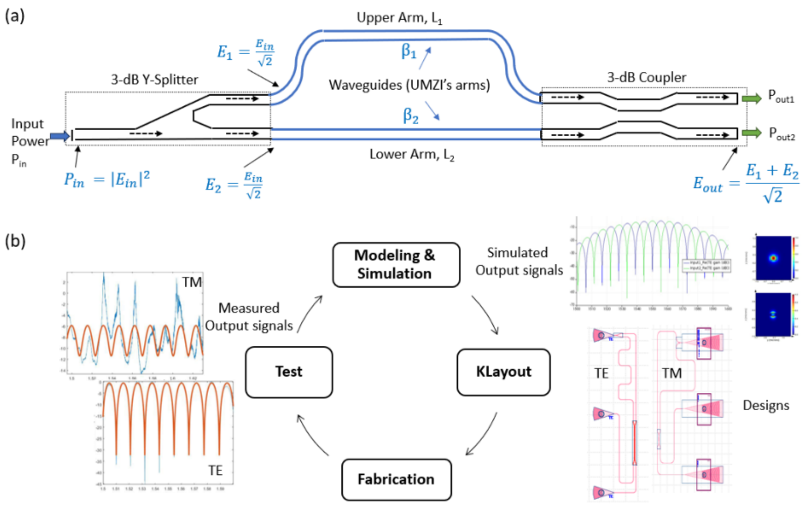

Fig. 1 (a) Schematic of unbalanced Mach-Zehnder interferometer that consists of two identical couplers and two arms: the upper arm with length L_1 and the lower arm with length L_2. The input optical signals $P_{in} = |E_{in}|^2$ is split equally using 3-dB Y-splitter, where the electrical field at upper and lower arms are $E_1 = \frac{E_{in}}{\sqrt{2}}$ and $E_2 = \frac{E_{in}}{\sqrt{2}}$, respectively. (b) PIC design cycle for photonic devices.

In our research, we have provided a comprehensive characterization of the UMZI structures for both polarization modes, namely the TE and TM modes of the UMZIs structures to report the fabrication variations on results due to imperfect forming of waveguide patterns due to sidewall roughness. This study provides a complete step-by-step phase with the results of the design cycle of a photonic device. The length difference between the two arms of the UMZI structure is studied with different cases varying from 50 µm to 250 µm by an increment of 50 µm, as in Table 1.

Table 1 Designs by varying UNZI 's arms lengths ΔL, where ΔL is changed by an increment of 50 µm for both TE and TM structures.

TE\TM designs ID	UMZI's Arms Difference (ΔL, μm)
MZI-1	50
MZI -2	100
MZI-3	150
MZI -4	200
MZI-5	250

Importantly, both experimental and simulation data are reported for the UMZI structure. The ultimate goal of our research is to study how the fabrication variation from different facilities could impact the performance of the UMZI structure, specifically, how the free spectrum range (FSR) and group index values are different than simulation results. Additionally, both TE and

TM modes are studied for the UMZI structures which provides a diverse investigation of the UMZI structure with respect to polarization. The TE designs are fabricated using electron beam lithography at UBC, and the TM designs are fabricated using photolithography at RIT. A silicon waveguide is used to layout the UMZI structure with typical dimensions, a width of 500 nm and a height of 220 nm. This research is structured as follows, Section 2 discusses the modeling and simulation of UMZI structure, Section 3 discusses the design layout, Section 4 shows the testing of experimental demonstration, Section 5 conclusion.

2. MODELING AND SIMULATION

2.1. Modes profile in Lumerical Mode solution

TE and TM waveguide mode for Si waveguide with 500 nm x 220 nm dimensions can be solved via Lumerical Solutions using finite difference eigenmodes solver as shown in Fig. 2 (Chrostowski and Hochberg, 2015, Chrostowski and Shoman, 2021, Saini et al., 2019).

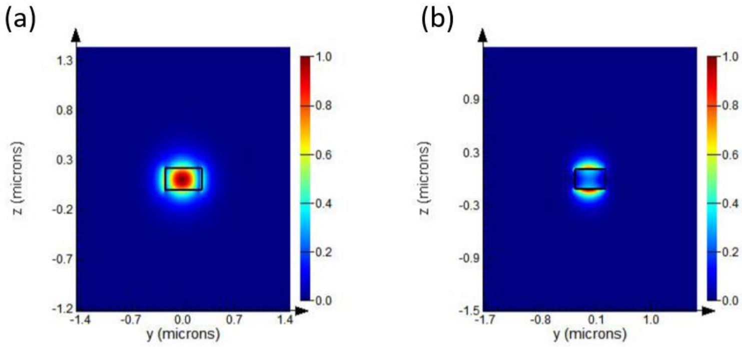

Fig. 2 The TE mode and TM mode profiles for a silicon waveguide (500 x 220 nm at 1550 nm) using Lumerical mode solution show the TE mode intensity is formed in the center, and the TM intensity is formed in the boundary of the waveguide.

The TE and TM mode profiles are solved using Lumerical mode solution (Finite Difference Eigenmode) as in the cross section view z y shown in Fig. 2 (a) and Fig. 2 (b) respectively. The silicon waveguide core has a refractive index of about 3.45, and the surrounding glass of silicon dioxide is around 1.45. The refractive index difference between the core and cladding of the Si-based waveguide enables a tight bend in design PICs due to the small critical angle of 24.8. This critical angle is calculated based on the total internal reflection of Snell's law theory.

2.2. Transfer Function of UMZI

The transmitted electric of a lossless unbalanced-MZI device can be obtained based on solving the following Matrix as in Eq. 1 and Eq.2 (Chrostowski and Hochberg, 2015):

$$[E_{out}] = [T_{coupler}][T_{Wgs}][T_{splitter}][T_{in}], \qquad (1)$$

$$\begin{bmatrix} E_{out1} \\ E_{out2} \end{bmatrix} = \begin{bmatrix} \sqrt{1-\varepsilon_2^2} & i\varepsilon_2 \\ i\varepsilon_2 & \sqrt{1-\varepsilon_2^2} \end{bmatrix} \begin{bmatrix} e^{-i\Phi_1} e^{\frac{-\alpha L_1}{2}} & 0 \\ 0 & e^{-i\Phi_2} e^{\frac{-\alpha L_2}{2}} \end{bmatrix} \begin{bmatrix} \varepsilon_1 \\ \sqrt{1-\varepsilon_2^2} \end{bmatrix} \begin{bmatrix} 0 \\ E_{in} \end{bmatrix}, \qquad (2)$$

where ε is coupling coefficient, ε^2 is the power split ratio, Φ is the accumulative phase, α is the propagation loss, L is the length of the Si waveguide. After computing transfer matrix multiplication, this yields the output electrical fields:

$$E_{out1} = i\varepsilon_2\sqrt{1-\varepsilon_1^2}\,e^{-i\Phi_1}e^{\frac{-\alpha L_1}{2}}E_{in} + i\varepsilon_1\sqrt{1-\varepsilon_2^2}\,e^{-i\Phi_2}e^{\frac{-\alpha L_2}{2}}E_{in}, \quad (3)$$

$$E_{out2} = -\varepsilon_1 e^{-i\Phi_1}e^{\frac{-\alpha L_1}{2}}E_{in} + \sqrt{1-\varepsilon_1^2}\sqrt{1-\varepsilon_2^2}\,e^{-i\Phi_2}e^{\frac{-\alpha L_2}{2}}E_{in}, \quad (4)$$

From the output electric fields, the mathematical model of the UMZI's output powers can be solved by $P = |E|^2 = EE^*$ that yields:

$$P_{out1} = P_{in}\left(e^{-\alpha L_1}(1-\varepsilon_1^2)\varepsilon_2^2 - 2e^{-\alpha L_1}e^{-\alpha L_2}\varepsilon_1\varepsilon_2\sqrt{1-\varepsilon_1^2}\sqrt{1-\varepsilon_2^2}\cos(\Delta\Phi_1) + e^{-\alpha L_2}(1-\varepsilon_2^2)\varepsilon_1^2\right), \quad (5)$$

$$P_{out2} = P_{in}\left(e^{-\alpha L_1}\varepsilon_1^2\varepsilon_2^2 + 2e^{-\alpha L_1}e^{-\alpha L_2}\varepsilon_1\varepsilon_2\sqrt{1-\varepsilon_1^2}\sqrt{1-\varepsilon_2^2}\cos(\Delta\Phi_2) + e^{-\alpha L_2}(1-\varepsilon_1^2)(1-\varepsilon_2^2)\right), \quad (6)$$

Where the phases terms $\left(\Delta\Phi_1 = \beta_1\Delta L = \frac{2\pi n_{eff1}}{\lambda_o}\Delta L\right)$ *and* $\left(\Delta\Phi_2 = \beta_2\Delta L = \frac{2\pi n_{eff2}}{\lambda_o}\Delta L\right)$ are the accumulative phase difference in the upper and lower arms, respectively. β is propagation of optical signal in the waveguides and n_{eff} is the effective refractive index. For identical couplers ($\varepsilon_1^2 = \varepsilon_2^2 = K$) the above equations can be simplified to yield:

$$P_{out1} = P_{in}\left(e^{-\alpha L_1}(1-K)K - 2e^{-\alpha L_1}e^{-\alpha L_2}K(1-K)\cos(\Delta\Phi_1) + e^{-\alpha L_2}K(1-K)\right), \quad (7)$$

$$P_{out2} = P_{in}(e^{-\alpha L_1}K^2 + e^{-\alpha L_1}e^{-\alpha L_2}2K(1-K)\cos(\Delta\Phi_2) + e^{-\alpha L_2}(1-K)^2). \quad (8)$$

The propagation loss α (dB/cm) in the upper arm is defined by $e^{-\alpha L_1}$,and the propagation loss in the lower arm is defined by $e^{-\alpha L_2}$. Typically, loss comes from imperfect waveguides due to fabrication variation, which leads to scattering the optical signals outside of the Si waveguide. For UMIZ design, the propagation loss exists in both arms; thus, for simplicity, can be assumed to be negligible, where $e^{-0L_1} = e^{-0L_2} = 1$, this yields:

$$P_{out1} = P_{in}\left((1-K)K - 2K(1-K)\cos(\Delta\Phi_1) + K(1-K)\right), \quad (9)$$

$$P_{out2} = P_{in}(K^2 + 2K(1-K)\cos(\Delta\Phi_2) + (1-K)^2). \quad (10)$$

The transfer function of the UMZI, transmittivity can be obtain by $T = \frac{P_{out}}{P_{in}}$ that yields:

$$T_1 = 2K(1-K)(1-\cos(\Delta\Phi_1)), \quad (11)$$

$$T_2 = K^2 + 2K(1-K)\cos(\Delta\Phi_2) + (1-K)^2. \quad (12)$$

The above UMZI transmittivity works for any power slit ratio K. The UMZI transmittivity in Eq. 11 is independent on the power slit ratio K, and it is dependent on the power slit ratio K only in Eq.12. Thus, when the power slit ratio K varies as function of wavelength as shown in Fig. 3(b), the exciton ratio (ER) varies as function of wavelength, the exciton ratio (ER) is defined the ratio between the maximum power and minimum power of the UMZI transmittivity in the linear scale.

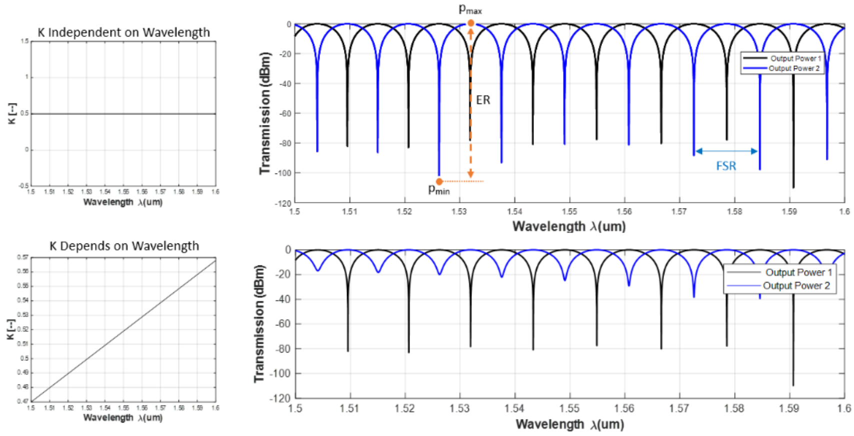

Fig. 3 (a) Imbalanced Mach-Zehnder interferometer transmission for ΔL= 50 µm for losses waveguides and ideal 3-dB couplers. (b) Imbalanced Mach-Zehnder interferometer transmission for ΔL= 50 µm for losses waveguides and non-ideal 3-dB couplers; this shows the UMZI transmittivity dependance on the power slit ratio K.

2.3. UMZI Simulation

The first stage in the photonic design cycle for modeling and simulation is discussed in this section for UMZI structure. UMZI designs are simulated using Lumerical Interconnect, as shown in Fig. 4. Designs are constructed by varying the length difference between the two arms of each UMZI, as in Table 1. The optical network analyzer is configured to generate optical power for a broadband wavelength of 1500 nm to 1600 nm and two input ports to measure the output of a UMZI device. The photonic couplers and Si waveguide are consistent with the fabricated designs; for example, the TE grating coupler (GC) is used in TE designs, and the TM grating coupler is used in TM designs. All of these subsystems (e.g., TE/TM couplers, TE/TM GCs, and Si waveguides) are loaded with S-parameters for lab data for each subsystem to exhibit the same performance as in actual lab operation. Fig. 5 shows an example of simulated data for the UMZI device with a length difference of 150 µm between the two arms. We can see obviously the TE output spectrum has smooth output power due to

the optimized TE GC (Zhang et al., 2013); there are no ripples in the peak power. The TM design spectrum shows imperfect smoothness in the output spectrum due to the fact that the TM GC is not fully optimized yet. Generally, both the TE and TM designs show the expected spectrum of the UMZI due to the interference phenomena.

Table 2 Free spectrum range (FSR) and group index per each UMZI design with a given arm lengths ΔL, where ΔL is changed for both TE and TM design.

Simulation		**TE UMZI**			**TM UMZI**		
Designs	ΔL(µm)	FSR (nm)	*ng*	λ (µm)	FSR (nm)	*ng*	λ (µm)
MZI1	50	11	4.33	1.5446	13	3.69	1.5502
MZI2	100	5.58	4.3	1.5503	6.4	3.75	1.5477
MZI3	150	3.748	4.27	1.5508	4.74	3.38	1.5485
MZI4	200	2.85	4.21	1.55	3.24	3.71	1.5505
MZI5	250	1.995	4.19	1.5501	2.696	3.56	1.5494

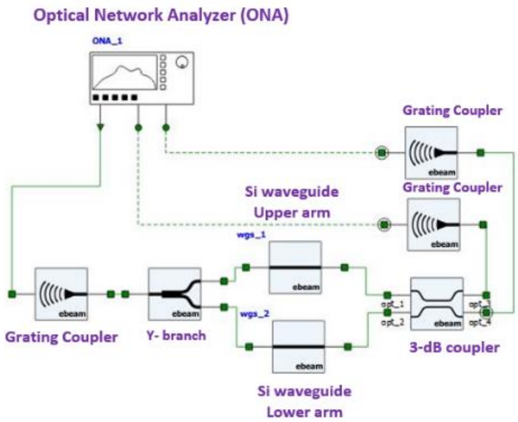

Fig. 4 Imbalanced Mach-Zehnder interferometer design using Lumerical Interconnect tool, optical network analyzer, grating couplers, Si waveguides, 3-dB coupler and Y-branch.

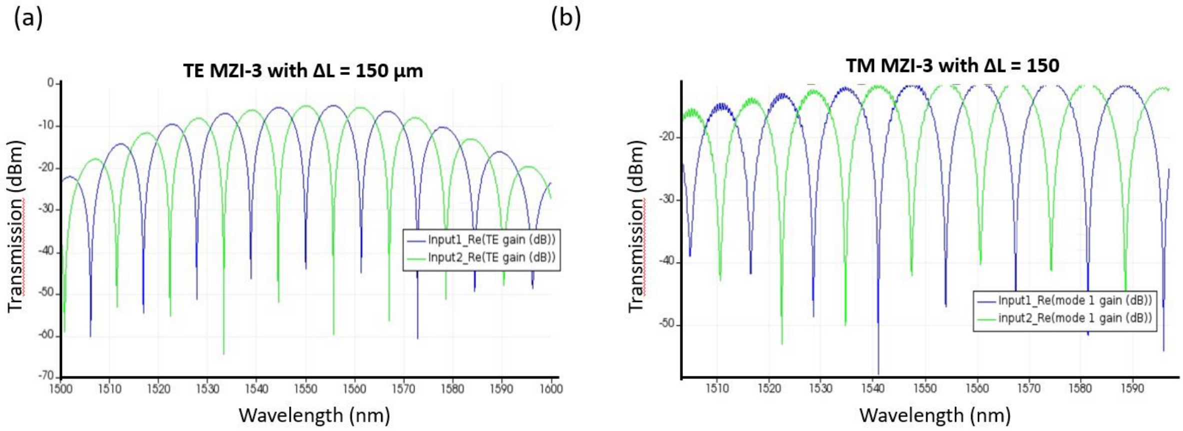

Fig. 5 Simulated output spectrum of UMZI arms' length difference of 150 µm (a) TE UMZI (b) TM UMZI.

3. DESIGNS LAYOUT

The next phase in the design cycle is the layout; the unbalanced Mach-Zehnder interferometer designs were drawn using KLayout software as shown in Fig. 6 based on Table 1, where only ΔL is varied.

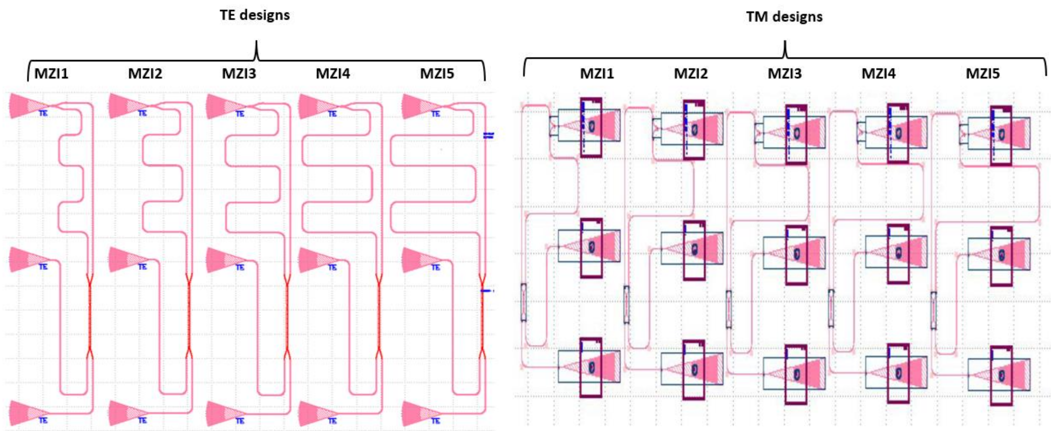

Fig. 6 The TE and TM designs in Klayout, the arm difference between the UZMI upper and lower arms, vary from 50 um to 250 um by an increment of 50 um. The TE design grating couplers are oriented to the right, and the TM grating couplers are oriented to the left as specified in the testing requirement for each polarization.

The KLayout software includes a Silicon Electronic-Photonic Integrated Circuits (SiEPIC) process design kit (PDK) that has a library with silicon photonics components in Compact Model Library (CML) (Chrostowski and Hochberg, 2015 and Bojko et al., 2011). The CML includes photonic subsystem components needed to draw the UMZI structure. For example, the CML waveguide model is named (ebaem-Wg-strip-1550), and the grading coupler (GC) is named (ebeam-gc-te-1550) by (Wang et al., 2014). A Y-branch with a 3-dB splitter and a 3-dB broadband directional coupler are used to combine the light from the two unbalanced MZI arms named (ebeam-bdc-te-1550). Furthermore, KLayout supports verification through design rule check and labels for automated testing. For instance, in the layout, the spacing between the GCs has to be 127 µm based on testing requirements.

4. TESTING OF EXPERIMENTAL DEMONSTRATION

4.1. Experiential Demonstration

UMZI designs are tested using PIC test station as illustrated in Fig. 7. The main components are the control and monitor unit, tunable laser source, fiber array, top view and side view cameras and illuminating light source, PIC stage, and optical power meters.

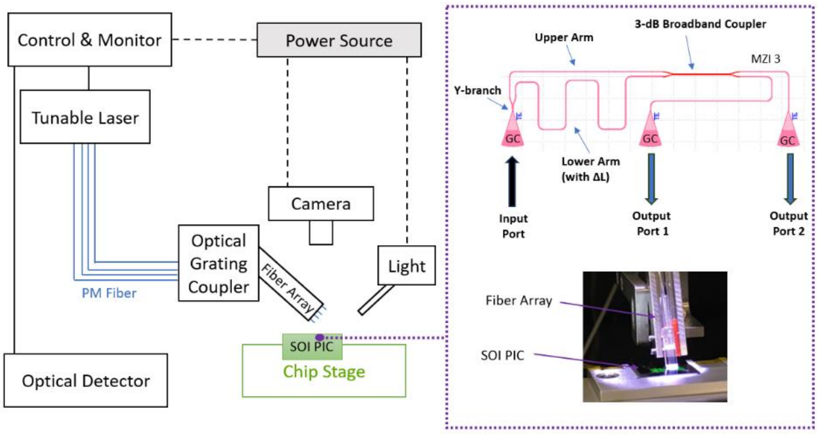

Fig. 7 The main part of the PIC test station consists of control and monitor units, the polarization-maintaining fiber array with four ports, a top-view camera and side-view camera, and a light source; each design has an input grating coupler (GC) and at least one output GC.

The tunable source launches polarized light through a PM fiber. The PM fiber maintains the input optical signal's polarization state into the PIC (to be either a TE mode or a TM mode). Then, the optical signals are coupled into the UMZI designs via vertical coupling through a fiber array; a fiber array stage is used to configure the angle and gap to optimize coupling efficiency. The spacing between fibers in the fiber array is 127 µm, which matches the spacing between the grating couplers for each UMZI design as shown in Fig. 7. Each UMZI design has one input port and two output ports; the input power enters through a Y-branch to split the optical signals into the UMZI's arms, optimized by (Zhang et al., 2013), and then a 3 dB broadband coupler is used to combine the optical signals, optimized by (Lu et al., 2015), where interference occurs to form the UMZI spectrum. The FSR and group index can be found based on the output spectrum as reported in the Table. 3.

Table 3 Free spectrum range (FSR) and group index per each UMZI design with a given arm lengths ΔL, where ΔL is changed for both TE and TM design.

Experiment		TE UMZI			TM UMZI		
Designs	ΔL(μm)	FSR (nm)	*ng*	λ (μm)	FSR (nm)	*ng*	λ (μm)
MZI1	50	11.2	4.246	1.55	13.5	3.103	1.55
MZI2	100	5.71	4.207	1.55	7.18	3.47	1.55
MZI3	150	3.83	4.186	1.55	5.34	3.423	1.55
MZI4	200	2.88	4.182	1.55	3.73	3.299	1.55
MZI5	250	2.3	4.179	1.55	2.8	3.4	1.55

4.2. UMZI fabrication variations due to Waveguide Roughness

The physical reason for having fabrication variations is the imperfect forming of waveguide patterns due to sidewall roughness as shown in Fig. 8. The FSR and group index values for different length difference of the UMZI's arms are slightly changed for the TE mode between the expediential findings and simulated results as shown in Fig. 8 (a) and (c), respectively. The FSR and group index show relatively higher changes between the expediential findings and simulated results as shown in Fig. 8 (b) and (d) due to fabrication variations. This roughness exhibits dimensional changes of the Si waveguide and variations in the effective refractive indices that lead to variations in the effective group indices of Si waveguides (Lee et al., 2000; Vieu et al., 2000; Tseng et al., 2003). A sidewall roughness is formed due to fabrication processes. This roughness introduces variations in the effective refractive indices and results in variations in the effective group indices of Si waveguides. The sidewall roughness causes a change in the dimensions of the waveguide and distortion in the desired pattern (Lee et al., 2000; Vieu et al., 2000; Tseng et al., 2003). Several studies have discussed the relationship between the design complexity and the manufacturing variability to characterize the accuracy performance limits of the current manufacturing methods (Khan et al., 2019). Other research focuses on working on these variations in the modeling stage to identify variations early to boost the robust photonic devices against fabrication variation (Xing et al., 2022).

4.3. UMZI Fabrication Variations via Corner Analysis

The corner analysis provides a robust method to check the fabrication variation and its direct effect on the UMZI transmission and FSR values. This analysis is achieved by changing the waveguide dimension for the ideal case of having a width of 500 µm and a height of 220 µm, as shown in Fig. 9 for five cases of both TE and TM UMZIs. The ideal case is the design target case with 500 x 220 µm, the first case is 510 x 223.1 µm, the second case is 510 x 215.3 um third case is 470 x 215.3 µm, and the forth case is 470 x 223.1 µm. Fig. 9 (a) shows the TE

UMZI transmittivity for these five cases and Fig. 9 (b) shows the TE UMZI FSR changes for each case. Fig. 9 (a) shows the TM UMZI transmission for these five cases and Fig. 9 (b) shows the TM UMZI FSR changes for each case. TM design has more changes comparing with TE designs because TM mode as shown in Fig. 2 is dormient in the edges of the waveguide and as a results it is more sensitive for fabrication variation as proved in our experimental finding.

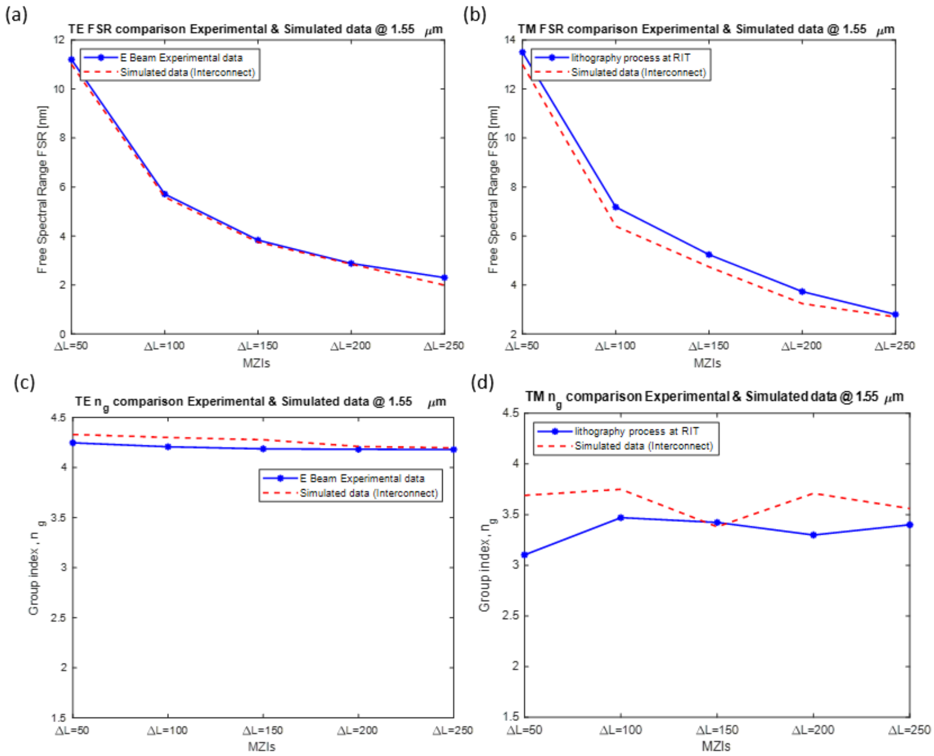

Fig. 8 The comparison between experimental results and simulation for the FSR and group index for each ΔL of the UMZI, (a) FSR for TE designs, (b) FSR for TM designs, (c) group index for TE designs, and (d) group index for TM designs.

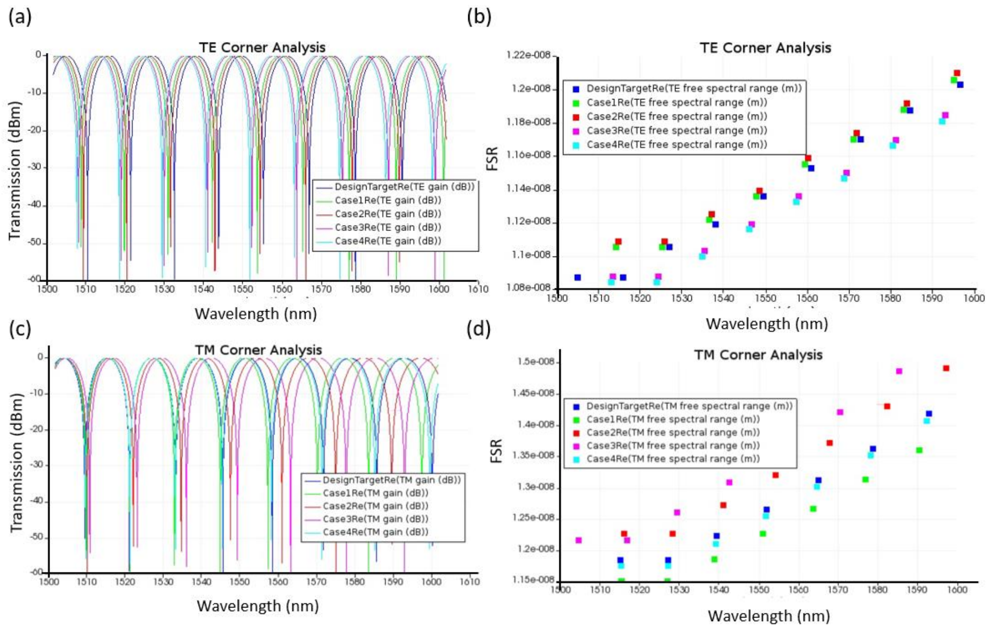

Fig. 9. Corner analysis for manufacturing variation for UMZI designs for ΔL= 50 µm, (a) TE transmission, (b) FSR for TE UMZI, (c) TM transmission, (D) FSR for TM UMZI.

5. CONCLUSION

UMZIs are experimentally measured for both the transverse electric (TE) and transverse magnetic (TM) modes. A UMIZ design consists of two 3-dB couplers and a Si waveguide to form the UMZI arms. When these arms are varied in length, causing a length difference ΔL. and the ΔL changes TE\TM of the UMZI's designs from 50 μm to 250 μm by an increment of 50 μm. TM designs are fabricated using photolithography at RIT, and the TE designs are fabricated using electron beam lithography at UBC. These two different fabrication facilities enable us to check design variation and compare the extracted free spectral range and group indices for each ΔL with simulation. The simulation such UMZI devices is studied to compare and verify the goodness of lab results. A slight variation in FSRs and group indices is observed between modeling and experimental results due to fabrication variation. For example, the group index for TE design exhibits slightly less variation for ΔL = 250 μm; as a result, this design might be used to investigate other applications using UMZI with ΔL = 250 μm, e.g., photonic sensing. The fabrication variations might affect high-performance applications; such applications are optical sensing and high-speed modulations that use UMZI structures especially for TM UMZI designs where it shows more variation than TE UMZI designs. Thus, in future research, group index variations and free spectral range are important factors to be considered and accounted. This work is focused on UMZI structure, and it is applicable to studying similar photonic structures (e.g., ring resonators) in photonic integrated circuits (PICs).

ACKNOWLEDGMENTS

I acknowledge Dr. Chrostowski, Dr. Stefan, and Dr. Maywar for the photonic integrated circuits courses, and the great opportunity of fabrication and automated testing. Many thanks to the Lumerical Solutions, Inc. team.

6. REFERENCES

AL-Zaidi, Z. and Sabbar, A. (2025) MICROWAVE PHOTONIC FILTERS BASED ON STIMULATED BRILLOUIN SCATTERING: A REVIEW. Kufa Journal of Engineering, 16(3).

Bojko, R.J., Li, J., He, L., Baehr-Jones, T., Hochberg, M. and Aida, Y. (2011) Electron beam lithography writing strategies for low loss, high confinement silicon optical waveguides. Journal of Vacuum Science & Technology B, 29(6).

Chrostowski, L. and Hochberg, M. (2015) Silicon photonics design: from devices to systems. Cambridge University Press.

Chrostowski, L. and Shoman, H., 2021, September. Online training in the design-fabricate-test of silicon photonic circuits. In Education and Training in Optics and Photonics (pp. F2B-3) Optica Publishing Group.

El Shamy, R.S., Afifi, A.E., Badr, M.M. and Swillam, M.A. (2022) 'Modelling, characterization, and applications of silicon on insulator loop terminated asymmetric Mach Zehnder interferometer', Scientific Reports, 12(1), 3598.

Khan, M.U., Xing, Y., Ye, Y. and Bogaerts, W. (2019) 'Photonic integrated circuit design in a foundry+ fabless ecosystem', IEEE Journal of Selected Topics in Quantum Electronics, 25(5), 1-14.

Lee, K.K., Lim, D.R., Luan, H.C., Agarwal, A., Foresi, J. and Kimerling, L.C. (2000) 'Effect of size and roughness on light transmission in a Si/SiO 2 waveguide: Experiments and model', Applied Physics Letters, 77(11), 1617-1619.

Liu, Q., Tu, X., Kim, K.W., Kee, J.S., Shin, Y., Han, K., Yoon, Y.J., Lo, G.Q. and Park, M.K. (2013) 'Highly sensitive Mach-Zehnder interferometer biosensor based on silicon nitride slot waveguide', Sensors and Actuators B: Chemical, 188, 681-688.

Lu, Z., Yun, H., Wang, Y., Chen, Z., Zhang, F., Jaeger, N.A. and Chrostowski, L. (2015) 'Broadband silicon photonic directional coupler using asymmetric-waveguide based phase control', Optics express, 23(3), 3795-3808.

Ndamati, I.T., Olayemi, O.S. and Madu, A.D. (2024) 'Demonstration of Interferometric Properties of Unbalanced Mach-Zehnder Interferometer', J. Eng. Res. Rep, 26(2), 145-155.

Saghaei, H., Elyasi, P. and Karimzadeh, R. (2019) 'Design, fabrication, and characterization of Mach-Zehnder interferometers', Photonics and Nanostructures-Fundamentals and Applications, 37, 100733.

Saini, S., Preble, S., Popović, M., Cardenas, J., Kost, A., Verlage, E., Howland, G. and Kimerling, L.C., 2019, May. Integrated photonics and application-specific design on a massive open online course platform. In Education and Training in Optics and Photonics (p. 11143_151) Optica Publishing Group.

Shoji, Y., Kintaka, K., Suda, S., Kawashima, H., Hasama, T. and Ishikawa, H. (2010) 'Low-crosstalk 2× 2 thermo-optic switch with silicon wire waveguides', Optics Express, 18(9), 9071-9075.

Sun, P. and Reano, R.M. (2010) 'Submilliwatt thermo-optic switches using free-standing silicon-on-insulator strip waveguides', Optics express, 18(8), 8406-8411.

Tapia-Licona, L.A., Vazquez, G.V., Rodriguez-Sevilla, E., Resendiz-Ramirez, R., Morales-Narvaez, E., Vazquez, R.M., Castro-Beltran, R. and Ramirez-Alarcon, R. (2025) 'Unbalanced

Mach-Zehnder interferometer fabricated by femtosecond laser direct writing for sensing of urea concentrations via evanescent field interaction', Optics & Laser Technology, 183, 112285.

Tseng, A.A., Chen, K., Chen, C.D. and Ma, K.J. (2003) 'Electron beam lithography in nanoscale fabrication: recent development', IEEE Transactions on electronics packaging manufacturing, 26(2), 141-149.

Tu, X., Liow, T.Y., Song, J., Luo, X., Fang, Q., Yu, M. and Lo, G.Q. (2013) '50-Gb/s silicon optical modulator with traveling-wave electrodes', Optics express, 21(10), 12776-12782.

Vieu, C., Carcenac, F., Pepin, A., Chen, Y., Mejias, M., Lebib, A., Manin-Ferlazzo, L., Couraud, L. and Launois, H. (2000) 'Electron beam lithography: resolution limits and applications', Applied surface science, 164(1-4), 111-117.

Wang, Y., Wang, X., Flueckiger, J., Yun, H., Shi, W., Bojko, R., Jaeger, N.A. and Chrostowski, L. (2014) 'Focusing sub-wavelength grating couplers with low back reflections for rapid prototyping of silicon photonic circuits', Optics express, 22(17), 20652-20662.

Xing, Y., Dong, J., Khan, U. and Bogaerts, W. (2022) 'Capturing the effects of spatial process variations in silicon photonic circuits', ACS Photonics, 10(4), 928-944.

Zhang, Y., Yang, S., Lim, A.E.J., Lo, G.Q., Galland, C., Baehr-Jones, T. and Hochberg, M. (2013) 'A compact and low loss Y-junction for submicron silicon waveguide', Optics express, 21(1), 1310-1316.